Princeton Plasma Physics Laboratory

PPPL- 4475

PPPL- 4475

Advances in High-harmonic Fast Wave Physics in the National Spherical Torus Experiment

G. Taylor, R. E. Bell, J. C. Hosea, B. P. LeBlanc, C. K. Phillips, M. Podesta, E. J. Valeo, J. R. Wilson J-W. Ahn, G. Chen, D. L. Green, E. F. Jaeger, R. Maingi, P. M. Ryan, J. B. Wilgen, W. W. Heidbrink, D. Liu, P. T. Bonoli, T. Brecht, M. Choi, and R. W. Harvey

December, 2009

PPPL
PRINCETON PLASMA PHYSICS LABORATORY

Prepared for the U.S. Department of Energy under Contract DE-AC02-09CH11466.

Advances in high-harmonic fast wave physics in the National Spherical Torus Experiment

G. Taylor, R. E. Bell, J. C. Hosea, B. P. LeBlanc, C. K. Phillips, M. Podesta,
E. J. Valeo, J. R. Wilson
Princeton Plasma Physics Laboratory, Princeton, New Jersey 08543, USA
J-W. Ahn, G. Chen, D. L. Green, E. F. Jaeger, R. Maingi, P. M. Ryan, J. B. Wilgen
Oak Ridge National Laboratory, Oak Ridge, Tennessee 37831, USA
W. W. Heidbrink, D. Liu
University of California, Irvine, California 92697, USA
P. T. Bonoli
Plasma Science and Fusion Center, MIT, Massachusetts 02139, USA
T. Brecht
University of Minnesota, Minnesota 55455, USA
M. Choi
General Atomics, San Diego, California 92186, USA
R. W. Harvey
CompX, Del Mar, California 92014, USA

Abstract

Improved core high-harmonic fast wave (HHFW) heating at longer wavelengths and during start-up and plasma current ramp-up, has now been obtained by lowering the edge density with lithium wall conditioning, thereby moving the critical density for perpendicular fast-wave propagation away from the vessel wall. Lithium conditioning allowed significant HHFW core electron heating of deuterium neutral beam injection (NBI) fuelled H-mode plasmas to be observed for the first time. Large edge localized modes were observed immediately after the termination of rf power. Visible and infrared camera images show that fast wave interactions can deposit considerable rf energy on the outboard divertor. HHFW-generated parametric decay instabilities were observed to heat ions in the plasma edge and may be the cause for a measured drag on edge toroidal rotation during HHFW heating. A significant enhancement in neutron rate and fast-ion profile were measured in NBI-fuelled plasmas when HHFW heating was applied.

PACS# 52.55.Fa, 52.35.Hr

I. INTRODUCTION

Many magnetically confined fusion devices, including ITER, rely on rf heating and current drive (CD) to provide bulk heating and to control plasma stability. High-harmonic fast wave (HHFW) research in the National Spherical Torus (NSTX) [1] is directed towards maximizing the core heating and CD efficiency by reducing power loss in the plasma edge and scrape off layer (SOL). In particular, HHFW experiments and modeling are motivated by the need for core heating and *q(0)* control during non-inductively sustained H-mode plasmas fuelled by energetic deuterium neutral-beam injection (NBI), as well as the need to provide HHFW-driven bootstrap current during solenoid-free plasma current ramp-up [2]. Recently, considerable progress has been made in improving the HHFW coupling and heating efficiency in ohmically-heated helium and deuterium target plasmas, and in H-mode deuterium target plasmas heated and fuelled by deuterium NBI, and the results from this research may have particular significance for ITER [3].

The 12-strap HHFW antenna in NSTX is located on the outboard midplane and extends 90^o toroidally. Six decoupled 30 MHz sources can provide up to 6 MW of rf power to the antenna. The antenna launches a well-defined spectrum of directed waves with launched toroidal wavenumbers, k_ϕ = ±13 m^{-1}, ±8 m^{-1} and ±3 m^{-1}, when the phase difference ($\Delta\phi$) between adjacent antenna straps is ±150^o, ±90^o and ±30^o, respectively [4, 5]. At other values of $\Delta\phi$ the antenna simultaneously launches several dominant spectral components. Lower k_ϕ waves should have higher CD efficiency, making k_ϕ = ±3 m^{-1} particularly attractive for CD in NSTX [2].

NSTX plasmas have a high ratio of plasma to magnetic pressure (β), typically the toroidal β = 10 - 40%. The high β causes strong single pass absorption of HHFW by electron Landau damping and transit-time magnetic pumping [1], even at the longest wavelengths that can be launched by the NSTX HHFW antenna (corresponding to k_ϕ = ±3 m^{-1}). Both the GENRAY [6] ray tracing and the AORSA [7] full wave codes predict very strong first-pass absorption in the HHFW regime in NSTX [8, 9] with the waves being almost entirely damped as they the pass through the high β core. Consequently, rf power losses in the plasma scrape-off and edge in the vicinity of the antenna, as opposed to multi-pass damping losses, play the critical role in limiting the heating efficiency in the plasma core.

There are several candidate processes that can contribute to rf power loss near the plasma edge, including parametric decay instability (PDI) heating via ion Bernstein wave excitation [10], and propagating and reactive wave-driven losses. It has also been observed in NSTX that when the edge density near the antenna is above the critical density for perpendicular fast wave propagation (n_{crit}) there is a reduction in core heating efficiency [8, 9] that is consistent with surface wave propagation near the antenna and the vessel wall, resulting in less rf power reaching the plasma core. A similar behavior is observed in conventional tokamaks at lower ICRF harmonics, where core heating efficiency is observed to be much lower with $\Delta\phi = 0^o$ phasing than with $\Delta\phi = 180^o$ phasing [11]. Here, n_{crit} is approximately proportional $k_{ll}^2 B/\omega$, where k_{ll} is the wavevector parallel to the magnetic field, B is the magnetic field and ω is the wave frequency. Earlier experiments on NSTX [8] had demonstrated improved HHFW heating efficiency in helium L-mode discharges by increasing B at the same k_ϕ [8]. Recently significant improvements in HHFW core heating efficiency were achieved by employing lithium conditioning [12] to reduce the edge density in order to move n_{crit} farther from the antenna and first wall [13, 14]. As a result core heating at lower k_ϕ was considerably enhanced and the first clear observation of $k_\phi = -3$ m^{-1} core electron and total heating in deuterium was obtained. This is a particularly notable achievement because, as mentioned earlier, the CD efficiency is expected to be much higher at low k_ϕ. Lithium conditioning has enabled record NSTX central electron temperatures, $T_e(0) > 5$ keV in deuterium and > 6 keV in helium with only ~3 MW of rf power at $k_\phi = -8$ m^{-1}. Lithium conditioning also resulted in the first significant core electron heating of deuterium NBI-fuelled H-mode plasmas. Most notably, coupling of rf power was maintained through the L-mode to H-mode (L-H) transition and was sustained even during H-modes with relatively large edge-localized modes (ELMs). These and other results obtained with lithium conditioning are presented in Section II.

Visible camera images of the antenna and visible and infrared camera images of the lower divertor region indicate that fast wave interactions can deposit considerable rf energy on the outboard divertor plate, especially for lower k_ϕ waves that begin to propagate closer to the vessel wall. Also, there is evidence that HHFW-generated PDI is heating ions in the edge and possibly driving them onto direct loss orbits that intersect the wall, and that this process may be the cause for an observed drag on toroidal rotation near the plasma edge during HHFW heating. During discharges with both HHFW and NBI heating there is an enhancement in the measured neutron rate, and fast-ion D_α (FIDA) emission diagnostic data [15] show significant enhancement and broadening of the fast-ion profile near the plasma core during HHFW heating. These observations clearly indicate a strong interaction between fast-waves and fast-ions. The FIDA signals have recently been compared to signals simulated by the CQL3D Fokker-Planck code [16, 17] and a finite-orbit simulation by the ORBIT-RF Monte-Carlo code [18]. The FIDA emission clearly shows fast-ion profile broadening that is much greater than predicted by Fokker-Planck modeling when HHFW power is applied to NBI-fuelled plasmas, pointing to the need for a full-orbit treatment in the simulation. Results on rf interactions with the plasma edge, divertor and fast-ions are presented in Section III.

Finally, the HHFW antenna was upgraded from a single to a double end-fed configuration. First results from this upgraded antenna show a higher arc-free power capability and are discussed in Section IV. A summary discussion of results and future plans is presented in Section V.

II. HHFW HEATING OF PLASMAS CONDITIONED WITH LITHIUM

Two lithium evaporators [12] have been used to inject collimated beams of lithium towards the lower divertor to apply lithium coatings on the graphite and carbon-fiber-composite plasma facing components in NSTX. These coatings have resulted in many beneficial effects [19], including contributing to improved HHFW electron heating in the plasma core by reducing the electron density in front of the antenna [14]. Figure 1 (a) shows the significant reduction in edge density, measured by multi-point laser Thomson scattering (MPTS), when lithium wall conditioning is added to deuterium plasmas heated by deuterium NBI (the plasma separatrix is located at R = 1.44 m in these discharges). The reduction in edge density produced by lithium conditioning moves n_{crit} away from the HHFW antenna (located at R = 1.58 m), reducing rf power coupling near the antenna and improving coupling to the plasma core. This has resulted in the production of plasmas with $T_e(0) > 5$ keV in deuterium (Figs. 1(b) and 1(c)) and $T_e(0) > 6$ keV in helium with only ~ 3 MW of rf power (Figs. 1(d) and 1(e)). These temperatures are particularly impressive for NSTX which operates at a maximum axial toroidal field, $B_T(0)$ of only 5.5 kG. The electron temperature profile ($T_e(R)$) became very peaked during rf heating, reaching $T_e(0) = 5.2$ keV in deuterium and $T_e(0) = 6.2$ keV in helium. $T_e(R)$ in deuterium is broader, with a steeper T_e gradient, probably due to the development of a reversed-shear q profile [20, 21]. The helium discharge eventually transitions to an H-mode plasma late in the rf heating pulse.

A scan of $\Delta\phi$ performed for series of deuterium L-mode plasmas with $I_p = 600$ kA, $B_T(0) = 5.5$ kG that had 1 MW of rf power starting at 0.15s, and without using lithium conditioning, shows a degradation in heating efficiency with decreasing k_ϕ (Fig. 2) that is similar to the degradation measured in helium L-mode discharges [9]. $\Delta\phi$ was stepped from -180^0 to -30^0 in 30^0 increments, and included a plasma with no rf power. $T_e(0)$, measured by MPTS, (Fig. 2(a)) rises faster for larger $\Delta\phi$ (higher k_ϕ). Note for the shot with $\Delta\phi = -30^0$ (k_ϕ= -3 m^{-1}) there was an arc in the rf antenna at 0.22 s causing a notch in rf power. But even before the rf power notch it is clear the rise in $T_e(0)$ is almost the same as the shot with no rf power. Figures 2(b) and 2(c) show $T_e(R)$ and electron density profile ($n_e(R)$) measured by MPTS at 0.382 s. Larger $\Delta\phi$ (higher k_ϕ) resulted in a more centrally peaked $T_e(R)$ and lower $\Delta\phi$ resulted in higher central electron density ($n_e(0)$) [8]. The central electron pressure, $P_e(0)$, was about the same for shots with $|\Delta\phi| > 60^0$, with $P_e(0)$ in the range 8.3-9.0 kPa. $P_e(0)$ decreased significantly for $|\Delta\phi| \leq 60^0$, so that $P_e(0) = 7.0$ kPa at $\Delta\phi = -60^0$ and $P_e(0) = 2.5$ kPa at $\Delta\phi = -30^0$.

Central electron heating at k_ϕ= -3 m^{-1} in NSTX was only observed in deuterium plasmas when lithium wall conditioning was employed to reduce the edge density. Figure 3 shows the time evolution of the line-integrated electron density (n_eL) measured by MPTS, the plasma stored energy, $T_e(0)$ measured by MPTS, and the rf power for two similar deuterium L-mode plasmas with 20 mg/min of lithium wall conditioning. Shot 129679 (solid line) had up to 1.3 MW of k_ϕ = -3 m^{-1} rf power. Shot 129677 (dashed line) had less than 150 kW of k_ϕ = -3 m^{-1} rf power (curtailed in time by arcs). There was a clear rise in plasma stored energy and n_eL at each rf pulse in shot 129679 relative to shot 129677. However, while $T_e(0)$ increased initially it fell before the end of each rf pulse. Since the density at the antenna was still above n_{crit} in this case, the heating efficiency in was still lower than at higher k_ϕ .

Lithium conditioning has also enabled the first observation of significant HHFW central heating during NBI-fuelled deuterium H-mode plasmas. Earlier attempts to couple HHFW power into deuterium NBI-fuelled H-mode plasmas in NSTX, without the benefit of lithium conditioning and at lower $B_T(0)$ = 4.5 kG, resulted in edge ion heating, but no core heating [22]. Figure 4 shows (a) $T_e(R)$, (b) $n_e(R)$ and (c) ($P_e(R)$) measured by MPTS at 0.482 s for two I_p = 1 MA, $B_T(0)$ = 5.5 kG deuterium plasmas. One of the discharges had 2 MW of NBI and 1.6 MW of rf power, with $\Delta\phi$ = 180^0 (k_ϕ = (14 + 18) m^{-1}), from 0.3 to 0.5 s (thick solid line, shot 129386), and the other discharge had only 2 MW of NBI (thin dashed line, shot 129381). There was a significant increase in $T_e(0)$ and $P_e(R)$ during the rf heating pulse.

The discharges in Fig. 4 benefited mostly from residual lithium coatings that had been laid down hours before and had minimal newly deposited lithium. H-mode plasmas heated by NBI, and conditioned with new lithium coatings that were replenished throughout the discharge, have been heated with 1.8 MW of k_ϕ= -13 m^{-1} and k_ϕ= -8 m^{-1} power (antenna launch spectra that can both heat and drive current). Electron heating was shifted off-axis and less heating was measured at k_ϕ = -8 m^{-1} than at k_ϕ = -13 m^{-1}, similar to the heating efficiency trend measured in L-mode plasmas [13]. About 66% of the rf power (~ 1.2 MW) was estimated to couple to the plasma at k_ϕ = -13 m^{-1}, and about 40% (~ 0.7 MW) was coupled at k_ϕ = -8 m^{-1}. MPTS edge density data indicated that the edge density was below n_{crit} for the case with k_ϕ = -13 m^{-1} heating but it was above n_{crit} for the case with k_ϕ = -8 m^{-1} heating.

Figure 5(a) shows the time history of the plasma stored energy for a plasma with k_ϕ = -13 m^{-1} heating (shot 130608, solid black line) compared to the background plasma with no rf heating (shot 130609, dashed black line). The rf pulse on shot 130608 turned off three times, the first two times because of an antenna arc (0.375 s and 0.437 s) and the third time during a programmed rf pulse shutdown (0.5 s). There was a clear rise in plasma stored energy during each rf pulse and at the end of each rf pulse there was a large type 1 ELM, indicated by the spike in divertor D_α emission (red line). Figure 5(b) shows an enlarged time window around the time of the arc at 0.375 s, the large ELM clearly followed the turn off of the rf pulse. Similarly, Fig. 5(c) shows that the large ELM followed the shut down of the rf power. Fast camera images prior to the growth of the ELM do not show the usual helical ELM structure [13]. Thus the ELM appears to be caused by the removal of the rf power via an arc or rf pulse turnoff. As will be seen in the next section, the edge rotation clamps during HHFW heating. It is possible then that the ELM is triggered when the edge rotation increases and the edge $E_r \times B$ shear changes after the rf power is turned off.

A challenge for coupling HHFW to H-mode plasmas is to maintain good coupling through the L-H transition and large ELMs that can significantly modify the edge density profile and change the separation between the antenna and the n_{crit} location. This can in turn lead to large changes in reflected power that can exceed the rf reflection coefficient trip level (typically set to 60-70% of the forward rf power) shutting down the rf sources. The issue here is not that 100% reflected power would damage the rf sources, but rather that there is a need to discriminate between reflections due to effects outside the antenna, and arcs in the antenna that could potentially lead to serious damage. Figure 6 shows data from an I_p = 800 kA, $B_T(0)$ = 5.5 kG deuterium plasma (shot 135340), conditioned with lithium, that was initially heated by 2 MW of NBI. An rf power of 2.7 MW at k_ϕ = -13 m^{-1} was applied from 0.25 to 0.46 s and an L-H transition occured soon after the start of the rf pulse at 0.29 s. Figure 6(a) shows the drop in divertor D_α emission at the time of the L-H transition followed by a sequence of D_α spikes during the ELMs. In this case rf power was sustained through the L-H transition and the ELMs. Figures 6(b) and (c) show MPTS $P_e(R)$ and $n_e(R)$ profiles at three times, just before (0.282 s) and after (0.298 s) the L-H transition and near the end of the rf pulse (0.432s). The edge density profile rapidly steepened at the L-H transition and $P_e(0)$ doubled during the rf pulse. Figure 6(d) shows the rf voltage reflection coefficient (blue) overlaid on the rf power waveform (black) and the divertor D_α signal (red). While there were large fluctuations in the reflection coefficient they only exceeded 0.3 briefly at the L-H transition in this case and never approached the trip level of 0.7.

Lithium wall conditioning also improved HHFW coupling during discharge startup and early plasma current ramp-up. This is particularly important because in solenoid-free scenarios, HHFW-generated bootstrap current ramp-up to I_p > 400 kA is needed to provide sufficient current to confine the 90 keV NBI ions in NSTX [2]. In recent experiments, k_ϕ = -8 m^{-1} rf power has been successfully coupled into lithium-conditioned deuterium plasmas at very low $T_e(0)$ and I_p. An rf power of 550 kW was coupled between 9 and 22 ms during the initiation of a discharge by Coaxial Helicity Injection (CHI) [23], increasing $T_e(0)$ from 3 to 15 eV when $n_e(0)$ ~ $4x10^{18}m^{-3}$. In addition, 550 kW of k_ϕ = -8 m^{-1} power was coupled from 20 to 64 ms into the early I_p ramp following CHI. Figure 7 shows (a) $T_e(R)$, (b) $n_e(R)$ and (c) $P_e(R)$ measured by MPTS at 52 ms for a plasma with rf power (solid line) and a similar plasma without rf power (dashed line). With the addition of rf power, $T_e(0)$ increased from 3 to 33 eV, $n_e(R)$ broadened and $n_e(0)$ increased by about 20%. As a result $P_e(0)$ increased by about an order of magnitude, although $P_e(R)$ remained hollow with $P_e(R)_{max}/P_e(0)$ ~ 2.

III. RF INTERACTION WITH PLASMA EDGE, DIVERTOR AND FAST-IONS

While surface wave losses can be reduced by edge conditioning techniques, such as lithium wall coatings, there is evidence of other detrimental rf power loss processes, particularly at lower k_ϕ. Previous passive spectroscopic ion temperature measurements for helium plasmas by the edge rotation diagnostic (ERD) [10] on NSTX indicated that PDI-generated ion Bernstein wave (IBW) ion heating may account for the loss of 16-23% of the rf power through ion collisions with poorly-confined edge electrons [24]. But the direct loss of PDI-generated energetic ions in the plasma edge may also be a significant loss channel for rf power. PDI-generated edge ion heating of carbon-III was measured during a sequence of similar I_p = 650 kA, $B_T(0)$ = 5.5 kG deuterium discharges with 1.2-1.3 MW of rf heating in which k_ϕ was changed from -13 m^{-1} to -3 m^{-1}. The poloidal edge ion temperature near the plasma separatrix (R ~ 1.5 m) was measured to increase with decreasing k_ϕ, as shown in Fig. 8(a), indicating increased rf power deposition in the edge region at lower k_ϕ. The ion heating became increasingly anisotropic as k_ϕ was reduced, with no change in toroidal ion temperature as k_ϕ was changed (Fig. 8(b)). Similar edge ion heating behavior was seen for carbon-VI, helium-II and lithium-II. The carbon-III poloidal ion temperature (Fig. 8(c)) and emissivity peaked at the plasma separatrix, whereas the carbon-III toroidal emissivity peaked outside the plasma separatrix, as shown in Fig. 8(d). A 1-D full wave model [25] was used to simulate the dependence of the amplitude of the PDI-generated IBW on the rf power for the range of k_ϕ values used in the experiment, and the results are summarized in Fig. 8(e). The model predicts that the threshold for PDI should fall with decreasing k_ϕ, as seen in the experiment, and that PDI should be generated with only ~ 100 kW of rf power at $k_\phi = 3$ m^{-1} and ~ 250 kW at $k_\phi = 13$ m^{-1}. So the rf power levels used in the experiment were well above the threshold levels expected to drive PDI.

Evidence for possible direct loss of PDI-generated energetic ions in the plasma edge is provided by charge exchange recombination spectroscopy (CHERS) [26] measurements of the plasma toroidal rotation velocity (V_{tor}) [13]. CHERS data were measured during a 40 ms, 2 MW NBI pulse that overlapped the end of the rf heating pulse by 30 ms during the antenna $\Delta\phi$ scan shown in Fig. 2. The CHERS measurements for carbon-VI V_{tor} at $R = 1.45$ m, just inside the plasma separatrix, during the antenna $\Delta\phi$ scan are plotted in Fig. 9(a). The edge V_{tor} slowed down more at lower $\Delta\phi$ (lower k_ϕ) and after the rf power is turned off V_{tor} immediately increased. Figure 9(b) shows the carbon-VI V_{tor} profiles measured by CHERS for the shot with $\Delta\phi = -60^0$. The profiles marked "10 ms", "20 ms" and "30 ms" are measured when the rf power was turned on. V_{tor} began to increase as the NBI imparted toroidal rotation to the core of the plasma, but V_{tor} near the edge remained clamped until the rf power was turned off, as indicated by the profile marked "40 ms". The black curve with the solid circles is the extrapolated V_{tor} profile before the NBI pulse was turned on. There was no toroidal rotation near the axis before the NBI pulse. The sudden relatively large increase in rotation near the plasma magnetic axis when the rf power was turned off suggests that rf heating also imposed a drag on core rotation. These results support the hypothesis that ions are gaining perpendicular energy from the PDI [10] and are then being ejected into the plasma scrape-off, increasing the electric field and possibly changing $E_r \times B$ shear in the edge. The large ELMs observed following the turn off of rf power in HHFW + NBI

H-modes, discussed in the last section, may be triggered by a change in edge $E_r \times B$ shear, but this remains to be established.

As discussed in the previous section, about a third of the rf power is estimated to be lost before it can couple to the core plasma of an HHFW + NBI H-mode for k_ϕ = -13 m^{-1} heating under the plasma conditions of Fig. 5, and this loss increases to about two-thirds for k_ϕ = -8 m^{-1} heating for similar conditions. While PDI-related mechanisms may account for some of this rf power loss it seems likely that there is a significant additional fast-wave power loss mechanism occurring in these H-mode discharges. Evidence for this mechanism is provided by visible color and infrared camera measurements, as shown in Fig. 10. Figures 10(a-c) show visible color camera images taken during three I_p = 1 MA, $B_T(0)$ = 5.5 kG deuterium H-mode plasmas. Image (a) is from a plasma that had only 2 MW of NBI heating (shot 130609). Images (b) and (c) are from plasmas that had 2 MW of NBI heating, but also had 1.8 MW of k_ϕ = -8 m^{-1} heating (shot 130621) and 1.9 MW k_ϕ = -13 m^{-1} heating (shot 130608), respectively. The images in frames (b) and (c) were taken at 0.335 s. Image (a) was taken at 0.350 s. An NBI-only background frame at 0.250 s in each shot was subtracted from each image to show differences in the image when HHFW power was applied. When rf heating was applied, power flowed along the magnetic field lines onto the lower outer divertor plate. This flow became much more prominent for the case with k_ϕ = -8 m^{-1} heating (Fig. 10(b)) than for the case with k_ϕ = -13 m^{-1} heating (Fig. 10(c)), in keeping with lower core heating efficiency at k_ϕ = -8 m^{-1}. Recently, dramatic evidence of the power densities associated with this interaction has been provided by calibrated infrared camera measurements of the lower divertor plates. Fig. 10(d) shows a plot of the heat flux versus major radius for two, H-mode discharges, one with 2 MW of NBI (black dashed line) and one with 2 MW of NBI and 2.6 MW of k_ϕ = -8 m^{-1} heating (red solid line). These discharges had a similar shape to the ones in Figs. 10(a-c). The heat flux to the lower outer divertor plate increased by about a factor of six at R = 0.98 m, to 3 MW/m^2 when rf heating was applied. Interestingly, recent 2-D AORSA modeling of NSTX HHFW plasmas, with the model boundary extended outside the plasma separatrix to the vacuum vessel wall [27], also predicts extensive rf electric fields in the scrape-off, particularly for k_ϕ = ± 3 m^{-1}

heating. This extended boundary modeling is now being incorporated into the 3-D AORSA simulation code.

GENRAY [6] modeling of the power deposition and partitioning between ions and electrons has been performed for recent deuterium HHFW + NBI H-mode discharges in NSTX. Results of this modeling are summarized for k_ϕ = -8 m^{-1} (shot 130621) and k_ϕ = -13 m^{-1} (shot 130608) heating in Fig. 11. The modeling results shown in Fig. 11 used the density and effective temperature for slowing NBI deuterium ions obtained from a TRANSP [28] time-dependent transport analysis of shot 130609, which is similar to shots 130608 and 130621, but without rf heating. HHFW power turns on at 0.25 s in shots 130608 and 130621 and the GENRAY analysis is performed at 0.353 s. At that time, in the case with k_ϕ = -8 m^{-1} heating, about 70% of the rf power is deposited on electrons and 30% is deposited on fast-ions (Fig. 11(a)). In the case with k_ϕ = -13 m^{-1} heating, about 85% of the rf power is deposited on electrons and 15% is deposited on fast-ions (Fig. 10(a)). When an NBI fast-ion population is not included in the GENRAY modeling over 95% of the rf power is predicted to couple to electrons for both rf cases. It is important to note here that the GENRAY modeling does not include rf acceleration of fast-ions. A TORIC [29] implementation in TRANSP, that also does not include a self-consistent treatment of the change in fast-ion population due to the rf acceleration of ions, shows a strong competition between electron and fast-ion damping in HHFW + NBI discharges that changes dynamically in time. A TORIC-TRANSP analysis of shot 130608 [30] predicts half the rf power is damped on fast-ions at the start of the rf pulse (0.25 s), falling to about 40% at the time of the GENRAY analysis (0.353 s) shown in Fig. 11(b), that is about a factor of three times higher than is predicted by GENRAY. These differences are being investigated.

Much of the rf power deposited on fast-ions in the core is expected to result in scattering of the ions into the banana loss region in the outer two-thirds of the plasma, so it is important to directly measure the spatial changes in the fast-ion profile in the presence of HHFW. There have been numerous studies of the interaction between fast-waves and fast-ions [31-35], however most of these studies were performed at fundamental or low ion cyclotron harmonics. In contrast, in the NSTX HHFW regime there are a large number of deuterium ion resonances simultaneously present in the plasma. Previously HHFW acceleration of NBI fast-ions was studied in NSTX with neutron counters and an E//B neutral particle analyzer (NPA) [35], which yielded almost no data on the spatial interaction between the fast-waves and the fast-ion population. With the installation of the FIDA [15] diagnostic on NSTX it has now been possible to measure the change in spatial distribution of fast-ions during HHFW heating [17]. Figures 12(a-c) show waveforms from a sequence of deuterium plasmas with 65 keV NBI blips (Fig. 11(a)). A 1.1 MW k_ϕ = -8 m^{-1} rf pulse is coupled from 0.15 to 0.4 s (Fig. 12(b)). Neutron measurements showed a clear enhancement due to rf acceleration of NBI fast-ions when shots with and without rf power were compared (Fig. 12(c)). Figure 12(d) shows a plot of the FIDA signal measured between 0.29 and 0.36s for three shots with rf (red line and symbols) and one shot with no rf (black line and symbols). The vertical green dashed lines indicate the major radial locations of the deuterium ion cyclotron resonances. There was a factor of two enhancement in the FIDA signal for the shots with rf power. The measured spatial profile was farther from the magnetic axis and broader than that predicted by the CQL3D Fokker-Planck code [17]. It appears that the finite Larmor radius and banana-width can have a significant effect on the fast ion profile in NSTX. To test this hypothesis, simulations with the ORBIT-RF finite-orbit Monte Carlo code coupled with the full-wave code AORSA and CQL3D with first order orbit width correction are in progress [18, 36].

IV. RECENT RESULTS FROM THE DOUBLE END-FED ANTENNA

Until the 2009 experimental campaign, the NSTX 12-strap HHFW antenna array had been coupled to the six rf transmitters by 12 antenna feeds connected to the top of each antenna strap [4, 5]. The bottom of each strap was connected to ground. Vacuum conditioning of the antenna in this configuration typically reached a system voltage limit ~ 25 kV, but when coupling to plasma the system voltage limit was typically ~ 15 kV. If the limit to the system voltage during plasma operation is set by the electric field in the vicinity of the straps and Faraday shield then it should be possible to increase the system voltage limit during plasma operation towards the vacuum voltage limit by reducing the electric field at the straps. To accomplish this, the straps were reconfigured with a ground in the center of each strap and a transmission line was fed to both the top and bottom of each strap. This reconfiguration included installing new antenna straps and entailed adding half-wavelength loops (~5 m long) between the top and bottom antenna feeds on each strap. These modifications, plus increasing some critical gaps by ~ 20-25%, were expected to reduce electric fields on the straps by about a factor of two and in the antenna box by about a factor of 1.4. Modifications to the transmission line components external to the vacuum vessel were accomplished during the early months of the 2009 run campaign when large amounts of lithium were being coated on internal vessel hardware, including the antenna. The upgraded antenna was operated during the last six weeks of the campaign, and initially the voltage limit for operation into vacuum was below 10 kV. However, the vacuum voltage limit was quickly increased to about 25 kV. Fast visible camera observations of the antenna during vacuum conditioning indicated that breakdowns were occurring in the antenna box, not in the transmission lines. When HHFW plasma operation was begun with the upgraded antenna, the previous rf power levels (2-3 MW) were achieved more quickly than during previous campaigns. Figure 13 shows fast TV camera images of the antenna taken at the start of the plasma conditioning at an rf power of 500 kW that clearly show material being ejected, including lithium, from the boron nitride between the straps and at the top and bottom of the antenna. Figure 13(a) is an image of the antenna showing strap locations under uniform plasma illumination. The camera image covers straps 1 through 9. Figures (b) and (c) show material being ejected from between straps 7 and 8 at the bottom of the antenna and from the top of the antenna between straps 7, 8 and 9. [A movie of the material ejections is available online as an enhancement to Fig. 13]. Arcs in the antenna were correlated with material ejections, although there were many ejections that did not cause arcs as in the case of Fig. 13. Arcs probably occur when particles enter the high rf electric field region inside the antenna Faraday shield.

The HHFW-heated plasma performance was significantly improved over previous run campaigns. Over 4 MW was coupled into a helium L-mode plasma, $T_e(0) > 6.2$ keV was achieved with only 2.7 MW of rf power and HHFW coupling was maintained through the L-H transition and during relatively large ELMs during deuterium NBI-fuelled H-mode discharges, as shown earlier in Section II. The improved performance and reliability of the new antenna also allowed a comprehensive study of the L-H and H-L transition in helium and deuterium plasmas using only ohmic and HHFW heating.

V. SUMMARY DISCUSSION AND FUTURE WORK

Improved core HHFW heating, particularly at longer wavelengths and during low-density start-up and plasma current ramp-up, has now been obtained by lowering the edge density with lithium wall conditioning. Significant core electron heating of NBI-fuelled H-modes has been observed for the first time over a range of launched wavelengths.

Visible and infrared camera images of the antenna and divertor indicate that fast wave interactions can deposit considerable rf energy on the outboard divertor plate, especially at longer wavelengths. Edge power loss was also occurring due to PDI-generated IBW that can drive ions out of the edge and onto direct loss orbits that intersect the wall, and that may be the cause for an observed drag on edge toroidal rotation in combined HHFW and NBI discharges. During plasmas where HHFW was combined with NBI, there was a significant enhancement in neutron rate and fast-ion D_α emission consistent with a strong interaction between the fast-waves and the NBI fast-ions. Comparison of the FIDA results with accurate physics-based modeling is essential in order to correctly interpret these data. As mentioned in Section III, differences between the FIDA measurements and a synthetic FIDA diagnostic [36] based on the present zero-orbit-width CQL3D Fokker-Planck and ORBIT-RF finite-orbit-width Monte Carlo simulations, support the conclusion that finite orbit-width effects need to be included in order to obtain agreement with the FIDA measurements [37]. A first order finite-orbit width correction is being added to the CQL3D code. However, fast ion orbit-widths in NSTX are often comparable to the plasma width, consequently a full-finite orbit width version of CQL3D is being implemented.

Large edge localized modes (ELMs) were observed immediately following the termination of rf power, whether the power turn off was programmed or due to antenna arcing. These ELMs may be destabilized by the change in edge $E_r \times B$ shear immediately following rf power turnoff. HHFW power was successfully applied during large ELMs by setting the source reflection coefficient trip levels to relatively high values – an approach potentially important for ITER ICRF heating if a method for discriminating between ELMs and arcs is also used. Recently the forward and reflected power data has been digitized on some plasmas with microsecond time resolution, rather than with the usual millisecond time resolution. The time derivative of the reflection coefficient obtained from this new high time resolution data was about an order of magnitude larger for an antenna arc than for an ELM and suggests that this signal can be used to effectively discriminate between changes in reflection coefficient due to arcs and ELMs. In 2010 the HHFW research program will use the upgraded antenna, with this ELM discrimination system, combined with a new liquid-lithium divertor [38], to study HHFW + NBI deuterium H-modes and to develop HHFW heating of the early I_P ramp-up.

ACKNOWLEDGEMENTS

This work would not have been possible without the support of Dr. Masayuki Ono and Dr. Jonathan Menard, the NSTX team, and the machine, rf, and neutral beam operations groups. The work is supported by US Department of Energy contracts DE-AC02-09CH11466 and DE-AC05-00OR2272.

REFERENCES

1. M. Ono, *et al.*, *Nuclear Fusion* **41**, 1435 (2001).
2. M. Ono, *Phys. Plasmas* **2**, 4075 (1995).
3. D. W. Swain and R. H. Goulding, *Fusion Eng. Des.* **82**, 603 (2007).
4. P. M. Ryan, *et al.*, *Plasma Physics and Controlled Fusion Research 2002*, Lyon, France (IAEA, Vienna, Austria 2003), paper EX/P2-13.
5. P. M. Ryan, *et al.*, Proc. 35th EPS Conf. on Plasma Physics (Hersonissos, Greece) paper P1.108 (2008).
6. A. P. Smirnov and R.W. Harvey, *Bull. Am. Phys. Soc.* **40**, 1837 (1995).
7. E. F. Jaeger, *et al.*, *Phys. Plasmas* **8**, 1573 (2001).
8. J. C. Hosea, *et al.*, *Phys. Plasmas* **15**, 056104 (2008).
9. C. K. Phillips, *et al., Nuclear Fusion* **49**, 075015 (2009).
10. T. M. Biewer, *et al.*, *Phys. Plasmas* **12**, 056108 (2005).
11. P. Colestock, *et al.*, *Fus. Eng. Des.* **12**, 43 (1990).
12. H. W. Kugel, *et al., Journal of Nuclear Materials* **390–391**, 1000 (2009).
13. J. C. Hosea, *et al.,* "*Recent Fast Wave Coupling and Heating Studies on NSTX, with Possible Implications for ITER*", to be published in AIP Proc. for 18th Topical Conf. on RF Power in Plasmas, (Gent, Belgium, June 2009).
14. G. Taylor, *et al.,* "*Recent Improvements in Fast Wave Heating in NSTX*", to be published in AIP Proc. for 18th Topical Conf. on RF Power in Plasmas, (Gent, Belgium, June 2009).
15. M. Podesta, *et al.*, *Rev. Sci. Instrum.* **79**, 10E521 (2008).
16. R. W. Harvey and M. G. McCoy, Proc. of IAEA Tech. Committee on Advances in Simulation and Modeling of Thermonuclear Plasmas, Montreal, Quebec (IAEA, Vienna, 1993), p. 489; USDOC NTIS Doc. No. DE93002962.
17. D. Liu, *et al.*, "*Profiles of Fast Ions that are Accelerated by HHFW in NSTX*", submitted to *Plasma Phys. and Control. Fusion* (2009).
18. M. Choi, *et al.*, *Phys. Plasmas* **12**, 1 (2005).
19. M. G. Bell, *et al., Plasma Phys. and Control. Fusion* **51**, 124054 (2009).
20. H.Y. Yuh, *et al.*, *Phys. Plasmas* **16**, 056120 (2009).

21. E. Mazzucato, *et al.*, *Nuclear Fusion* **49**, 055001 (2009).
22. B. P. LeBlanc, *et al.*, *AIP Conf. Proc.* **787**, 86 (2005).
23. R. Raman, *et al.*, *Nuclear Fusion* **49**, 065006 (2009).
24. J. R. Wilson, *et al.*, *AIP Conf. Proc.* **787**, 66 (2005).
25. G. Chen, *et al.*, *"AORSA-1D Simulation of Parametric Decay Instability (PDI) in Tokamak Plasmas" Bull. Am. Phys. Soc.* **54**, 71 (2009).
26. R. E. Bell, *Rev. Sci. Instrum.* **77**, 10E902 (2006).
27. D. L. Green, *et al.*, *"Self-Consistent Simulations of RF Heating in the Ion Cyclotron Range of Frequencies" Bull. Am. Phys. Soc.* **54**, 70 (2009).
28. R. J. Hawryluk, in *Physics of Plasmas Close to Thermonuclear Conditions*, *Proc. of the International School of Plasma Physics*, (edited by B. Coppi, G. Leotta, D. Pfirsch, R. Pozzoli, and E. Sindoni, Pergamon, Varenna, Italy, 1981), Vol. 1, p. 19.
29. M. Brambilla, *Plasma Phys. Control. Fusion* **44**, 2423 (2002).
30. B.P. LeBlanc, *et al.*, "*Analysis of High-Te Plasmas Heated by HHFW in NSTX* ", to be published in AIP Proc. for 18th Topical Conf. on RF Power in Plasmas, (Gent, Belgium, June 2009).
31. W. W. Heidbrink and G. J. Sadler, *Nuclear Fusion* **34**, 535 (1994).
32. M. Nemoto, *et al.*, *Plasma Phys. Control. Fusion* **39**, 1599 (1997).
33. W. W. Heidbrink, *et al.*, *Nuclear Fusion* **39**, 1369 (1999).
34. M. J. Mantsinen, *et al.*, *Phys. Rev. Lett.* **88**, 105002 (2002).
35. A. L. Rosenberg, *et al.*, *Phys. Plasmas* **11**, 2441 (2004).
36. W. W. Heidbrink, *et al.*, *Plasma Phys. Control. Fusion* **48**, 1347 (2006).
37. M. Choi, *et al.*, "*Iterated Finite Orbit Monte Carlo Simulation with Full Wave Fields for Tokamak ICRF Wave Heating Experiments*", to be submitted to *Phys. Plasmas* (2010).
38. H. W. Kugel, *et al.,* Plasmas **15**, 056118 (2008).

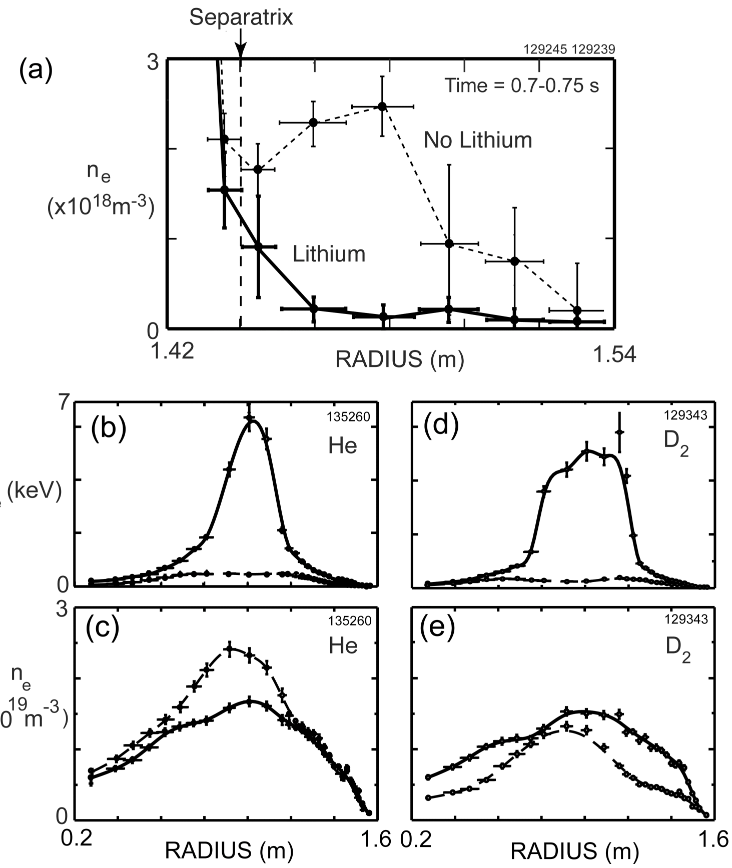

Figure 1

(a) Time averaged MPTS $n_e(R)$ in the plasma scrape-off between 0.7 and 0.75 s for two similar plasmas, one with lithium conditioning (shot 129254, thick error bars and solid thick line) and one without lithium conditioning (shot 129239, thin error bars and dashed line). Plasma separatrix is at R = 1.44 m and the HHFW antenna Faraday shield is located at R = 1.58 m. MPTS (b) $T_e(R)$ and (c) $n_e(R)$ immediately prior to rf heating (0.198 s, dashed line) and during 2.7 MW of $k_\phi = -8\ m^{-1}$ heating (0.298 s, solid line) of a helium plasma (shot 135260). MPTS (d) $T_e(R)$ and (e) $n_e(R)$ immediately prior to rf heating (0.148 s, dashed line) and during 3.1 MW of $k_\phi = -8\ m^{-1}$ heating (0.248 s, solid line) of a deuterium plasma (shot 129343).

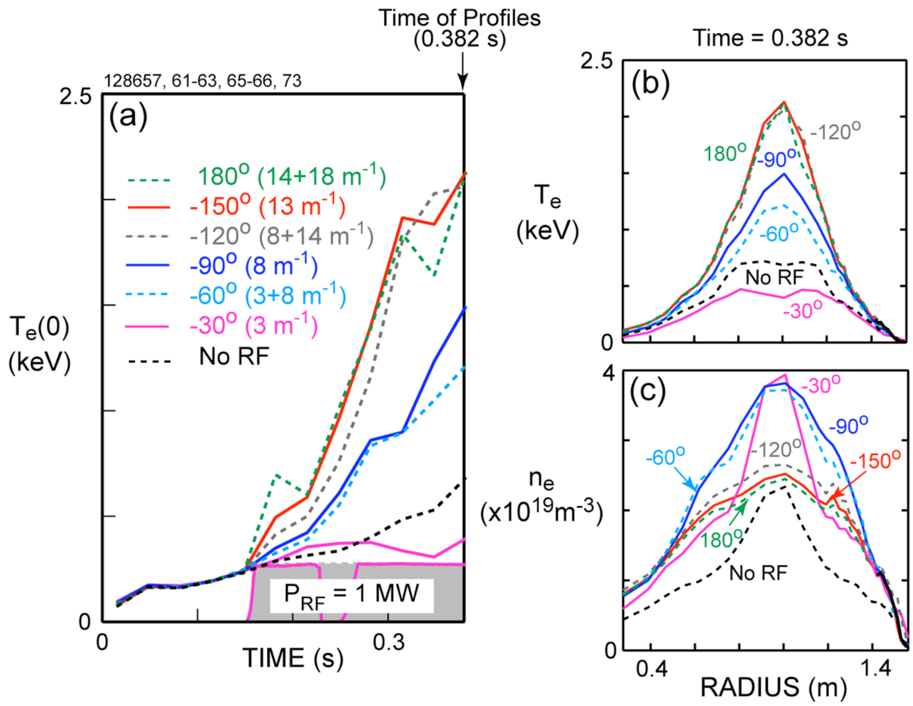

Figure 2

(a) Time evolution of the $T_e(0)$, measured by MPTS, for a sequence of deuterium plasmas with I_p = 600 kA, $B_T(0)$ = 5.5 kG, 1 MW of rf power starting at 0.15 s, and no Li conditioning. $\Delta\phi$ was adjusted from -30^0 to 180^0 in 30^0 increments between shots. $T_e(0)$ time evolution for a plasma without rf heating (black dashed line) is also plotted for comparison. Note the plasma with $\Delta\phi = -30^0$ had an rf arc at 0.22 s. (b) $T_e(R)$ and (c) $n_e(R)$ measured by MPTS at 0.382 s during each discharge shown in Fig. 2(a).

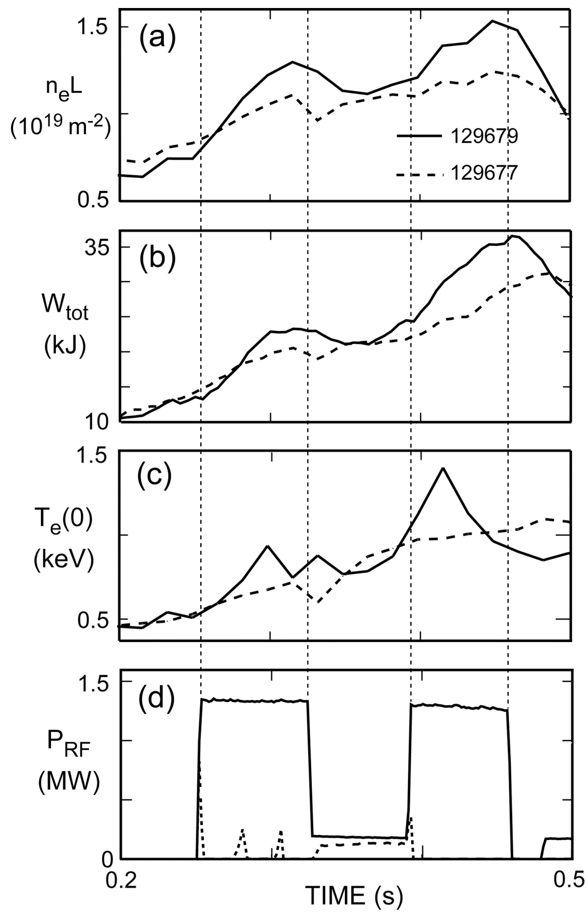

Figure 3

Time evolution of (a) n_eL measured by MPTS, (b) plasma stored energy, (c) $T_e(0)$ measured by MPTS, and (d) rf power for two similar deuterium L-mode plasmas with 20 mg/min of lithium wall conditioning. Shot 129679 (solid line) had up to 1.3 MW of k_ϕ = -3 m^{-1} rf power. Shot 129677 (dashed lines) had less than 150 kW of k_ϕ = -3 m^{-1} rf power.

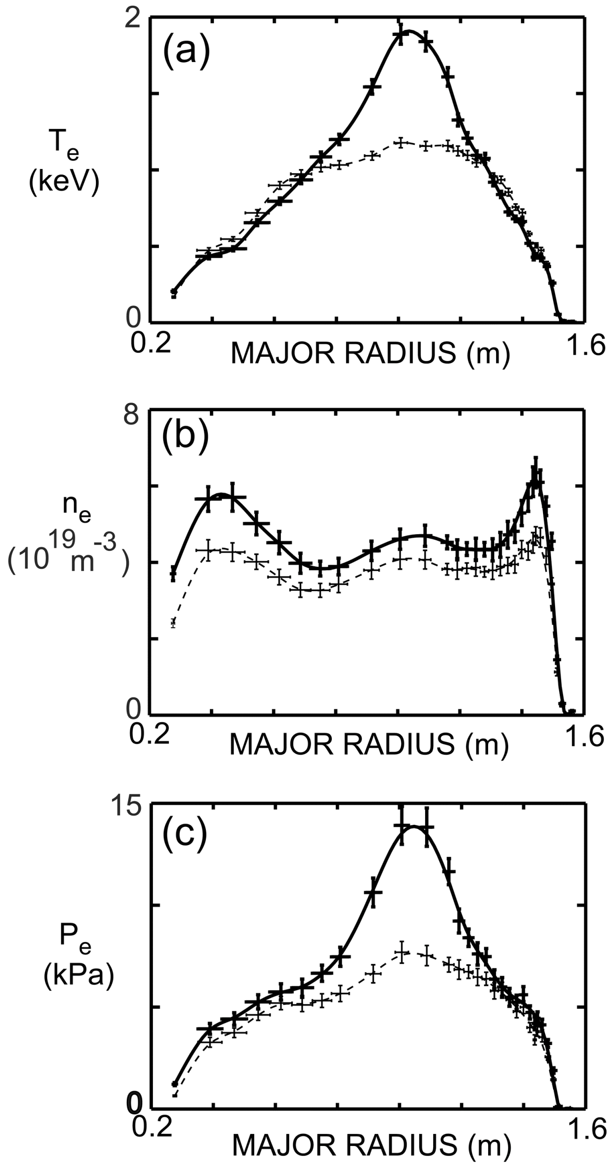

Figure 4

(a) $T_e(R)$, (b) $n_e(R)$ and (c) $P_e(R)$ measured by MPTS at 0.482 s for two I_p = 1 MA, $B_T(0)$ = 5.5 kG deuterium plasmas. One discharge had 2 MW of NBI and 1.6 MW of rf power, with $\Delta\phi = 180^0$ (k_ϕ = (14 + 18) m^{-1}), from 0.3 to 0.5 s (thick solid line, shot 129386), and the other discharge had 2 MW of NBI from 0.09 to 0.69 s (thin dashed line, shot 129381).

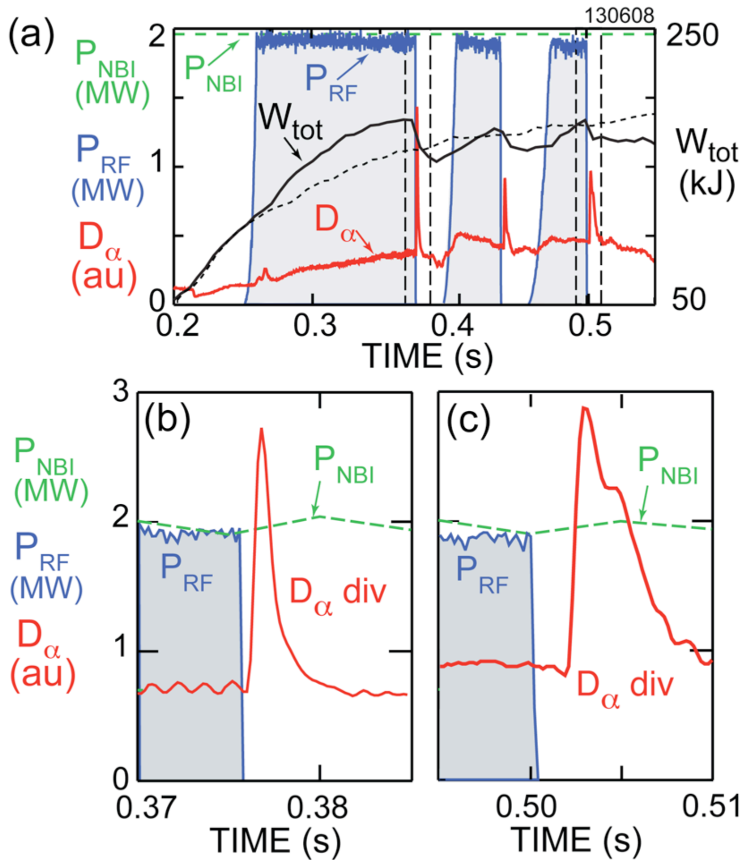

Figure 5

(a) Time evolution of rf power (blue line), NBI power (dashed green line), plasma stored energy (solid black line) and lower divertor D_α emission (red line) during an I_p = 1 MA, $B_T(0)$ = 5.5 kG deuterium NBI H-mode plasma with k_ϕ = -13 m^{-1} heating (shot 130608). The time evolution of the plasma stored energy for a similar plasma, but without rf heating (shot 130609), is shown by the dashed black line. rf power trips off during an antenna arc at 0.375 s and 0.437 s, and is turned off at 0.5 s, in each case there is a large D_α spike associated with a type 1 ELM. (b) Expanded time window around the time of the arc at 0.375 s, and (c) around the time of the rf turn-off at 0.5 s.

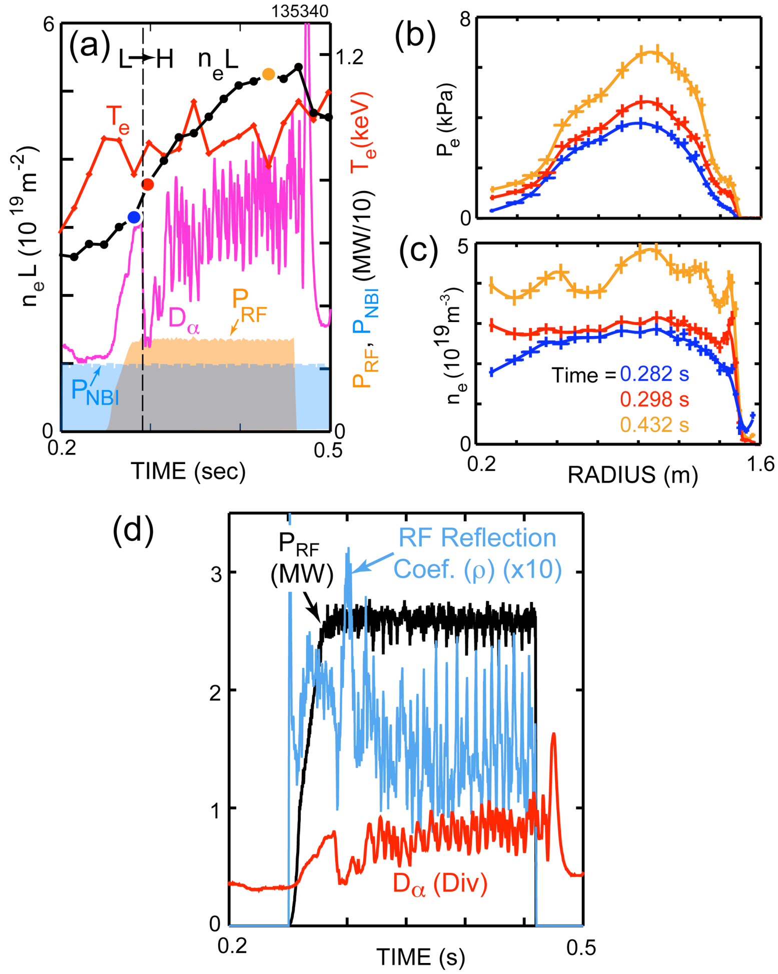

Figure 6

(a) Time evolution of the $T_e(0)$, n_eL, rf and NBI power, and the lower divertor D_a emission during an I_p = 800 kA, $B_T(0)$ = 5.5 kG deuterium plasma (shot 135340) iheated by 2 MW of NBI that transitions to an ELMing H-mode during the rf pulse at 0.29 s. This plasma had 2.7 MW of $k_\phi = -13\ m^{-1}$ heating from 0.25 to 0.46 s. (b) $P_e(R)$ and (c) $n_e(R)$ measured by MPTS just before (0.282 s, blue line) and after (0.298 s, red line) the L-H transition, and at the end of the rf pulse (0.432s, orange line). (d) rf power (black line), rf voltage reflection coefficient (blue line) and lower divertor D_a emission (red line) during shot 135340.

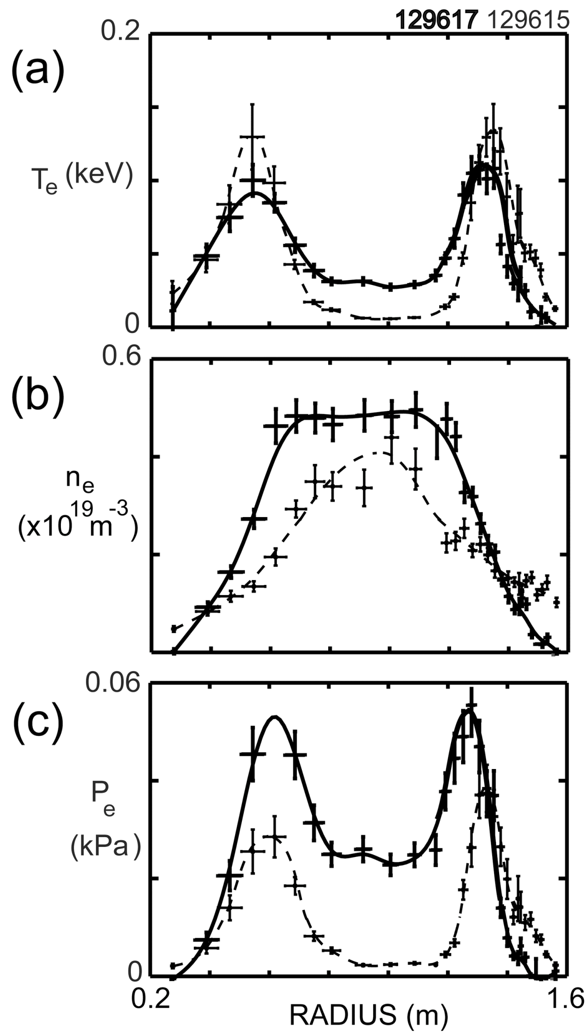

Figure 7

(a) Electron temperature, (b) electron density and (c) electron pressure profiles measured by MPTS for two $B_T(0)$ = 5.5 kG deuterium plasmas at 0.052 s, during the beginning of the current ramp-up. One discharge has 550 kW of k_ϕ = -8 m^{-1} heating coupled from 0.02 s (thick solid line) and the other discharge has no rf coupled (thin dashed line).

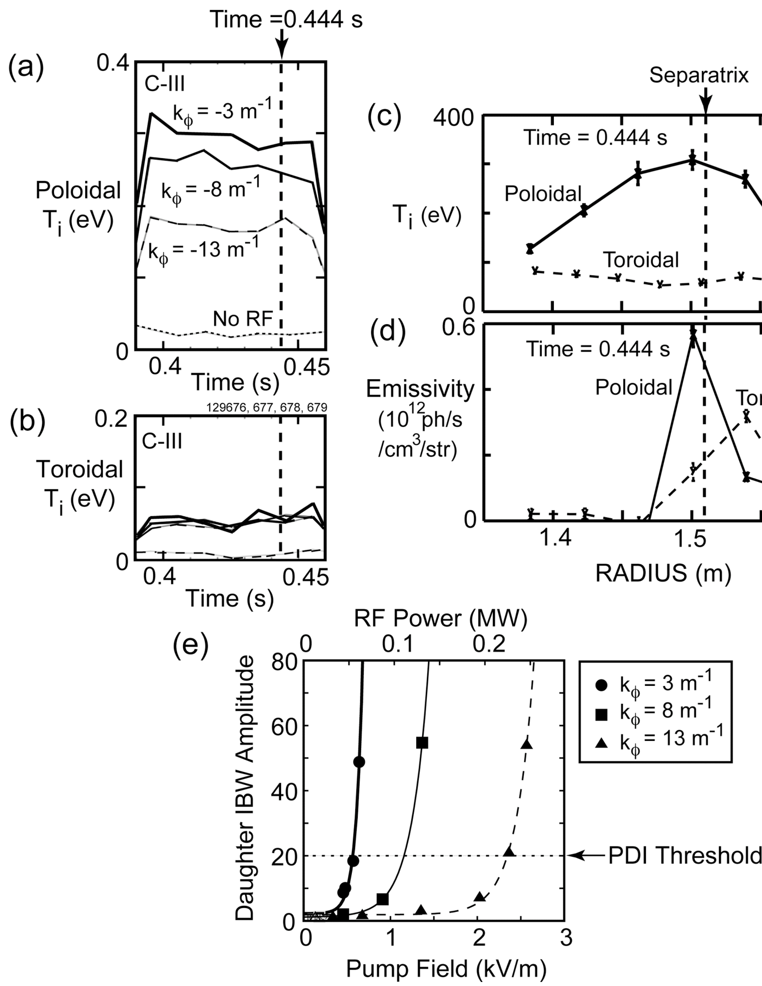

Figure 8

Anisotropic carbon-III ion heating measured near the plasma separatrix by passive ion spectroscopy. (a) Poloidal ion temperature at a major radius, R = 1.500 m and (b) toroidal ion temperature at R = 1.507 m, during 1.2-1.3 MW of k_ϕ = -3 m^{-1} (thick solid line, shot 129679), k_ϕ = -8 m^{-1} (thin solid line, shot 129678), k_ϕ = -13 m^{-1} (dashed solid line, shot 129676) rf heating of I_p = 650 kA, $B_T(0)$ = 5.5 kG deuterium discharges. Also included is a shot with no rf power (shot 129677, dotted line). For the case with k_ϕ = -3 m^{-1} heating at 0.444 s, radial profiles of (c) Poloidal (solid line) and toroidal ion temperature (dashed line), and (d) poloidal (solid line) and toroidal (dashed line) carbon-III emissivity. (e) Results from a 1-D full wave model of the PDI-generated IBW amplitude versus pump field and rf power.

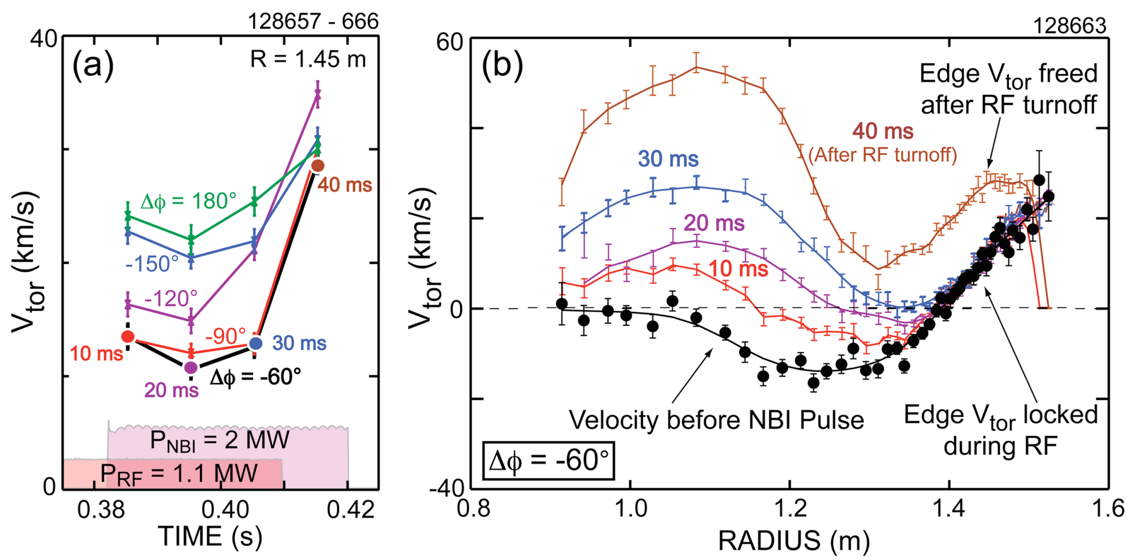

Figure 9

(a) Toroidal velocity of carbon-IV measured at R = 1.45 m by CHERS during a short 2 MW NBI at the end of a 1.1 MW rf pulse for the $\Delta\phi$ = -60^0 to -180^0 scan shown in Fig. 2. (b) Toroidal velocity of carbon-VI versus major radius for the $\Delta\phi$ = -60^0 rf heating case shown in Fig. 9(a) and Fig. 2.

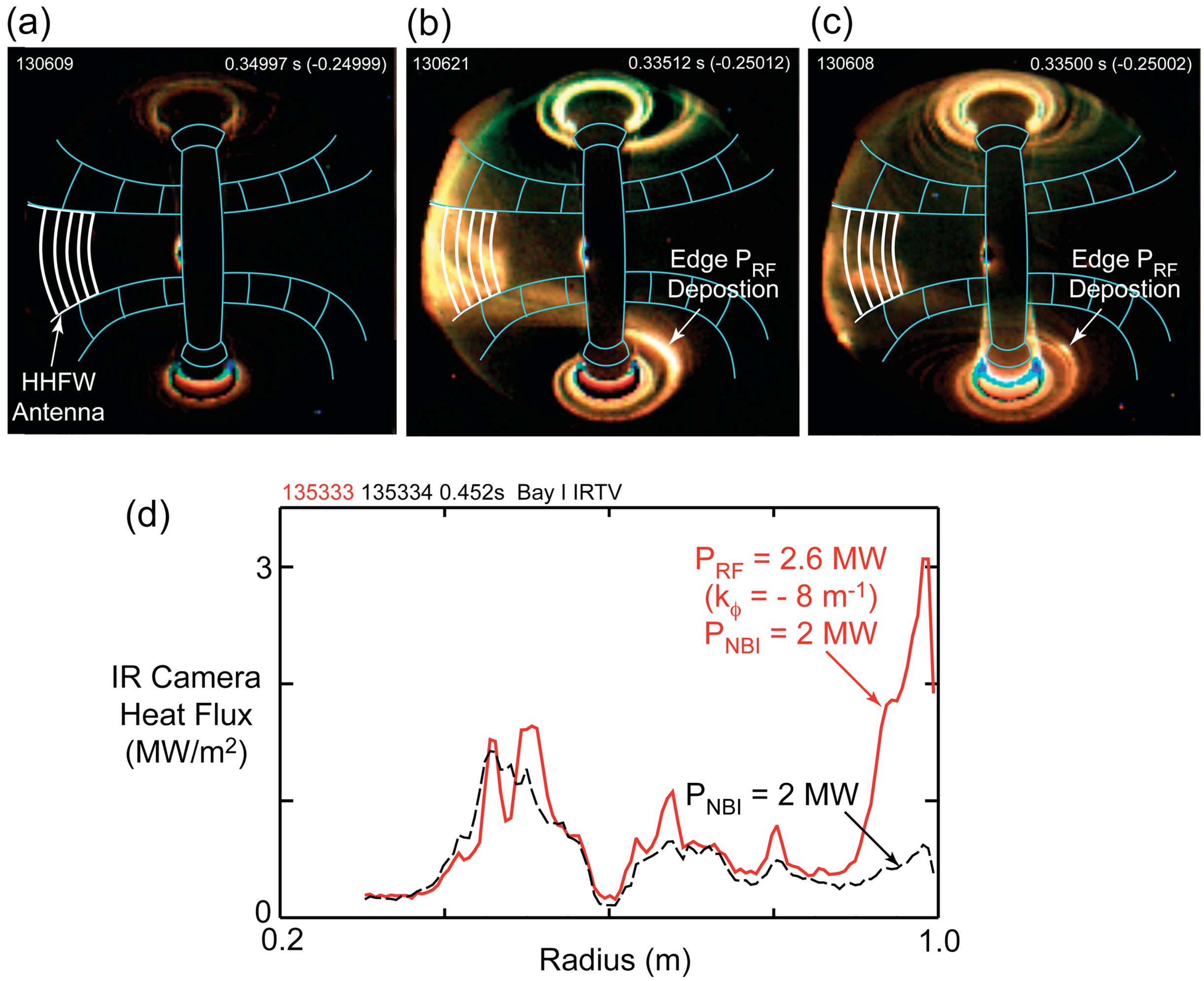

Figure 10

Visible color camera images taken during three I_p = 1 MA, $B_T(0)$ = 5.5 kG deuterium H-mode plasmas. (a) For plasma with only 2 MW of NBI heating (shot 130609). (b) and (c) For plasmas with 2 MW of NBI heating and 1.8 MW of k_ϕ = -8 m^{-1} heating (shot 130621) and 1.9 MW k_ϕ = -13 m^{-1} heating (shot 130608), respectively. (d) Radial heat flux measured by an IR camera viewing the lower divertor plate during two I_p = 800 kA, $B_T(0)$ = 4.5 kG deuterium H-mode plasmas, one with 2 MW of NBI (shot 135334, dashed black line) and the other with 2 MW of NBI and 2.6 MW of k_ϕ = -8 m^{-1} heating (shot 135333, red solid line).

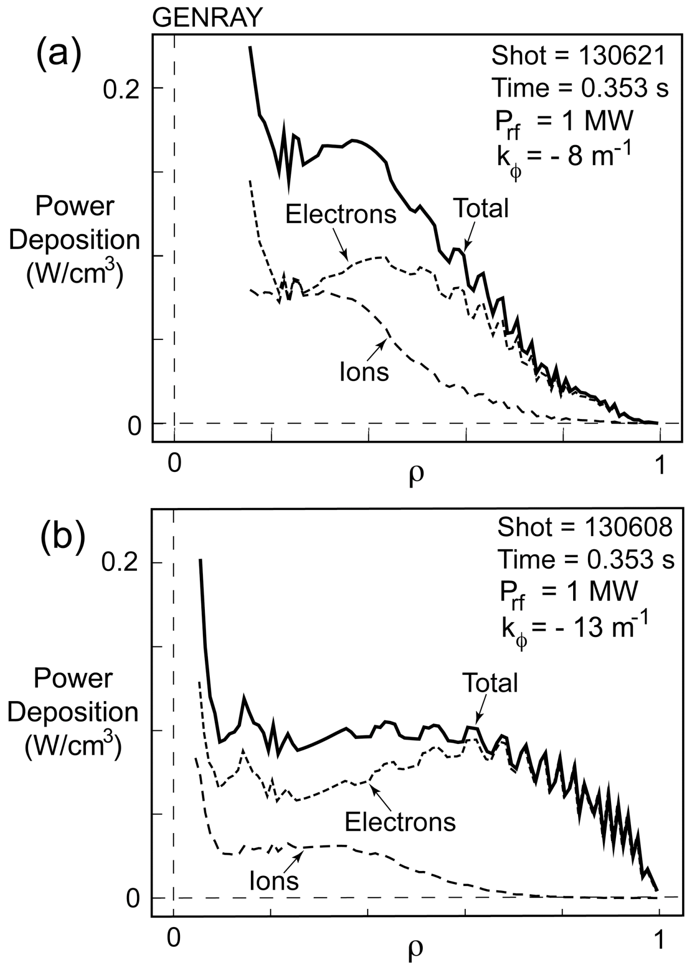

Figure 11

Power deposition profiles calculated by GENRAY for I_p = 1 MA, $B_T(0)$ = 5.5 kG deuterium H-mode plasmas with 1 MW of (a) k_ϕ = -8 m^{-1} (shot 130621) and (b) k_ϕ = -13 m^{-1} heating (shot 130608).

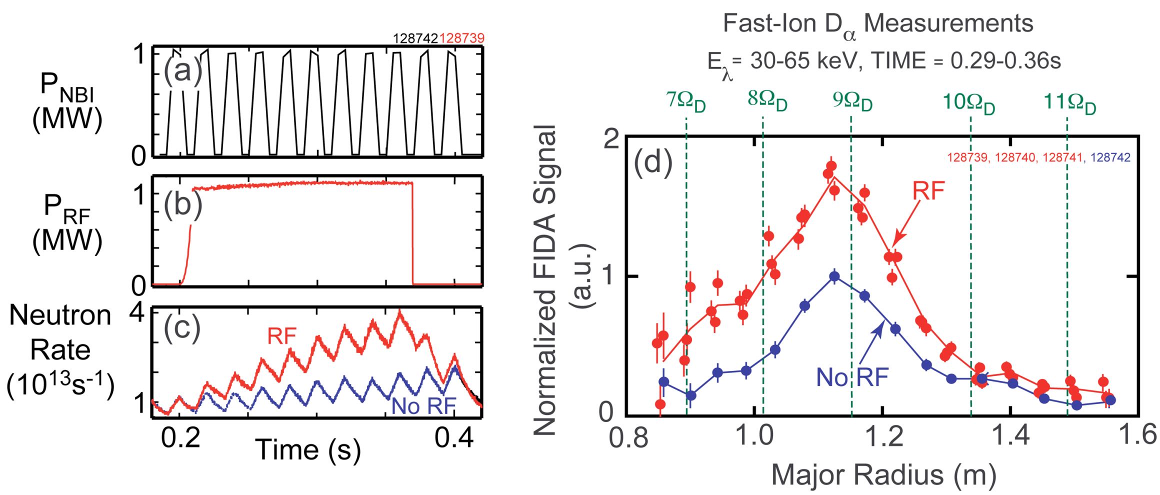

Figure 12

(a) Time evolution of a series of short 65 keV NBI blips for two similar I_p = 800 kA, $B_T(0)$ = 5.5 kG for two similar shots 128742 and 128739. (b) k_ϕ = -8 m^{-1} rf heating pulse for shot 128739. (c) Comparison between the measured neutron rates for shot 128739 (rf + NBI, red line) and shot 128742 (NBI, black line). (d) FIDA signal versus major radius during the time window 0.29-0.36 s for three similar plasmas with k_ϕ = -8 m^{-1} rf heating and NBI blips (shots 128739, 128740 and 128741, red line and symbols) and a similar plasma with only NBI blips (shot 178742, blue line and symbols).

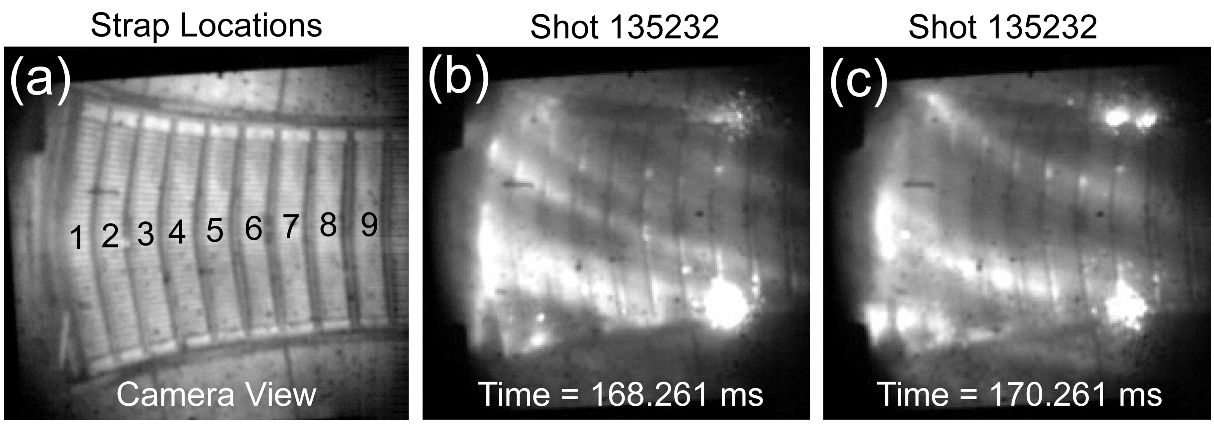

Figure 13

Visible camera image (a) showing strap locations under uniform plasma illumination, and (b) and (c) showing material being ejected from the antenna during plasma condition with 500 kW of rf power.

The Princeton Plasma Physics Laboratory is operated
by Princeton University under contract
with the U.S. Department of Energy.

Information Services
Princeton Plasma Physics Laboratory
P.O. Box 451
Princeton, NJ 08543

Phone: 609-243-2245
Fax: 609-243-2751
e-mail: pppl_info@pppl.gov
Internet Address: http://www.pppl.gov